Journal of Computational Physics **175,** 1–11 (2002)
doi:10.1006/jcph.2001.6963, available online at http://www.idealibrary.com on IDEAL®

A Comparison of Spectral and Vortex Methods in Three-Dimensional Incompressible Flows

Georges-Henri Cottet,* Bertrand Michaux,* Sepand Ossia,† and Geoffroy VanderLinden*,‡

*LMC–IMAG, Université Joseph Fourier, B.P. 53, 38041 Grenoble Cedex 09, France; †LEGI–IMG, Université Joseph Fourier, B.P. 53, 38041 Grenoble Cedex 09, France; and ‡Department of Mechanical Engineering, Université Catholique, 1348 Louvain la Neuve, Belgium

Received September 11, 2000; revised October 8, 2001

We present a comparison of the performance of vortex and pseudospectral methods in two reference flows: a homogeneous turbulent flow at low Reynolds number and a vortex reconnection case at a moderate Reynolds number. The results should contribute to a better understanding of the accuracy of vortex methods in both resolved and underresolved simulations. © 2002 Academic Press

Key Words: vortex and particle method; spectral method; isotropic turbulence; vortex reconnection.

1. INTRODUCTION

Spectral and vortex methods are numerical methods of a seemingly very different nature. On the one hand, spectral methods can be considered as a reference technique, highly accurate but limited to very specific geometries, at least for straightforward implementation. On the other hand, particle methods—vortex methods in the case of incompressible flows—are in general viewed as numerical *models*, merely able to give qualitative informations on flows, but naturally adapted to complex geometries.

However, developments of new tools in the last decade, concerning in particular the treatment of diffusion and boundary conditions, in many aspects, bring particle methods closer to conventional grid-based methods. Systematic comparisons with centered finite-difference schemes for a variety of two-dimensional flows (see Ref. [9]) have demonstrated that vortex methods compare well to nondissipative schemes in terms of accuracy. At the same time, vortex methods retain their adaptivity and robustness. They are free of any convection-related stability conditions, which permits use of large time steps. In many cases, this can lead, for a given accuracy, to substantial savings in computational time over grid-based solvers.

0021-9991/02 $35.00
Copyright © 2002 by Academic Press
All rights of reproduction in any form reserved.

This paper aims at achieving new quantitative information about the vortex method accuracy in two- and three-dimensional configurations, by means of systematic confrontation with pseudospectral methods. Our goal is not to undertake a convergence study for either method, but rather to address the following question: for a given flow and grid-size, what accuracy can be expected from these methods? **Au: as meant?**

The first test case deals with the classical direct numerical simulation (DNS) of homogeneous isotropic turbulence. The second one is the instability generated by two antiparallel vortex tubes. In the later case, our simulations were underresolved, as it is often the case in practice, and we wanted to investigate the subgrid behavior of vortex methods. We thus compared vortex methods with pseudospectral methods which either were dealiased or involved a subgrid dissipation model.

2. RESULTS

We first briefly sketch the numerical methods considered. We then describe the results of the simulations for the two flows under consideration.

2.1. *The Spectral and Vortex Codes*

We have focused on a geometry where both methods were straightforward to implement, namely a periodic box. The pseudospectral code used in our simulations is rather classical. Derivatives are computed in the Fourier space.

The nonlinear convective terms are expressed in their rotational form and are computed in the physical space, using Fast Fourier Transforms (FFTs). Time-stepping is performed using a third-order Runge–Kutta scheme. When appropriate, dealiasing was performed using the two-thirds rule [1].

The vortex code operates on the velocity–vorticity formulation of the Navier–Stokes equations. It is a time-splitting algorithm alternating advection and diffusion steps. The advection step consists of tracking particles of vorticity and updating their circulation to take into account the stretching. To compute the velocity field, two strategies are available for vortex methods. The first one is based on the Biot–Savart law. It requires the use of fast multipole expansions for N-body solvers. To the best of our knowledge, even the latest implementations of these solvers in three dimensions lead to computational costs which are several orders of magnitude larger than grid-based Poisson solvers. We thus elected the second strategy, which relies on the use of a Poisson solver on an underlying Eulerian grid. In this class of so-called vortex-in-cell (VIC) methods, the advection step goes through the following sequence of operations:

- Particle vorticity is interpolated to the grid.
- The stream function is calculated on the grid by a FFT-based Poisson solver.
- Velocity and stretching is computed by fourth-order centered finite difference on the grid, then interpolated back to the particle locations.
- Particles are pushed and their circulations are updated.

This sequence is repeated in a second-order Runge–Kutta scheme. This is essentially the VIC method of Christiansen [2], except for the interpolation kernel, which in our case is a third-order piecewise cubic spline. More precisely, the interpolation of vorticity onto the

grid is given by the formula

$$\boldsymbol{\omega}_i = \frac{1}{\Delta^3} \sum_p \boldsymbol{\Gamma}_p \boldsymbol{\Phi}\left(\frac{\boldsymbol{x}_i - \boldsymbol{x}_p}{\Delta}\right),$$

where Δ is the grid size and $\boldsymbol{x}_i$, $\boldsymbol{x}_p$, $\boldsymbol{\omega}_i$, and $\boldsymbol{\Gamma}_p$ are, respectively, the grid points, particle locations, grid vorticity and particle circulations. The kernel $\boldsymbol{\Phi}$ is obtained by tensor product of the following one-dimensional function:

$$\phi(x) = \begin{cases} 0 & \text{if } |x| > 2, \\ \frac{1}{2}(2-|x|)^2(1-|x|) & \text{if } 1 \le |x| \le 2, \\ 1 - \frac{5x^2}{2} + \frac{3|x|^3}{2} & \text{if } |x| \le 1. \end{cases}$$

At the end of the advection step particles are remeshed on a regular lattice through the same interpolation kernel. It should be noted that the choice of this nondissipative kernel plays an important role in the accuracy of the overall algorithm. In all our calculations the particle spacing is equal to the grid size, and the particles and grid points are laid on staggered grids. The diffusion is finally achieved by redistributing vorticity among nearby particles, through the finite-difference-like formula

$$\frac{d\boldsymbol{\Gamma}_p}{dt} = \nu \Delta^{-2} \sum_q (\boldsymbol{\Gamma}_q - \boldsymbol{\Gamma}_p) \Lambda\left(\frac{\boldsymbol{x}_p - \boldsymbol{x}_q}{\Delta}\right),$$

where

$$\Lambda(\boldsymbol{x}) = \begin{cases} \frac{6}{17}\frac{1}{1+|\boldsymbol{x}|^2} & \text{if } |\boldsymbol{x}| < 2, \\ 0 & \text{if } |\boldsymbol{x}| \ge 2. \end{cases}$$

Note that this results in a 27-point formula, which is in the spirit of the so-called particle strength exchange scheme [5]. However the particle remeshing prior to the diffusion step avoids quadrature-type error, which is in general associated with these diffusion solvers. Implementation details and numerical analysis of the various steps of the algorithm can be found in Refs. [5, 9]. It should be noted that the grid calculation of the velocity on the grid allows the numerical cost of the algorithm to be kept at a reasonable level. The Lagrangian character of the method is maintained in the transport of the particles and, as a result, the time step remains independent of the grid size. The time step is chosen to be proportional to min $(\|\boldsymbol{\omega}\|^{-1}, \|\boldsymbol{\nabla} : \boldsymbol{u}\|^{-1})$, which is the time scale over which the particles are subject to strain and rotation.

2.2. *DNS of Isotropic Turbulence (Run 1)*

In this experiment, a DNS of freely decaying isotropic turbulence is performed (see, for example, Ref. [7]). The initial velocity field has a Gaussian distribution and zero mean, with a kinetic-energy spectrum $E(k, 0) \propto k^4 \exp[-\frac{2k^2}{k_p^2}]$, where $k_p = 4$. Time is expressed in terms of large-eddy turnover time units L_0/u_0, where L_0 is the initial integral scale and $u_0^2 = \frac{2}{3}\langle \boldsymbol{u}(0)^2 \rangle$. The Reynolds number based on the Taylor microscale is initially 98 and decreases to 26 at $t = 8$. It should be noted that the duration of these

simulations exceeds the establishment of the self-similar cascade, which approximately occurs at $t = 4.5$ [6]. Calculations were performed in the periodic box $[0, 2\pi]^3$ with 128^3 collocation points or particles. As a result, 64 Fourier modes are considered in each direction of Fourier space, between $k_{min} = 1$ and $k_{max} = 64$. It was checked that at each instant the resolution requirement $k_{max}/k_d \geq 1.3$ was fulfilled, where k_d denotes the Kolmogorov dissipative wavenumber. Moreover, since in this case exponential decay of spectra started not later than wavenumber $\frac{2}{3}k_{max}$, the dealiasing threshold for spatial resolution $(2k_{max})^3$, the pseudospectral simulation was not dealiased. In other words, for the given grid resolution the spectral results can reasonably be considered as reference results.

Figure 1 shows the time evolution of the energy spectra obtained by the vortex and spectral methods. The difference in the tails of the spectra results in a less pronounced peak in the enstrophy curve for the vortex method (Fig. 2). Further comparisons indicate that the truncation errors induced in remeshing the particles are primarily responsible for the enstrophy deficit in the vortex method (see Ref. [11] for extensive comparisons; Refs. [4, 11] can be downloaded from www.lmc.imag.fr/lmc-edp/Georges-Henri.Cottet/). All other statistics usually computed for this type of flow are otherwise very close. Figure 3 shows the evolution of the skewness factor of $-\partial u_1/\partial x_1$, which is known to be a nondimensional measure of the kinetic-energy transfer. The agreement is rather good, in particular in the early stages of the computations, when the skewness undergoes a rapid variation. The probability distributions of the velocity and pressure (Fig. 4) are also in excellent agreement. By inspecting 3D visualizations of the vorticity modulus at different times, it was also checked that both simulations produce coherent structures in qualitative agreement. Figure 5 shows the vorticity isosurfaces corresponding to about 40% of the maximum vorticity at five turnover times. From these results one may recognize that the vortex-method simulation not only reproduces the statistical properties of the pseudospectral run, it yields deterministic agreement as well.

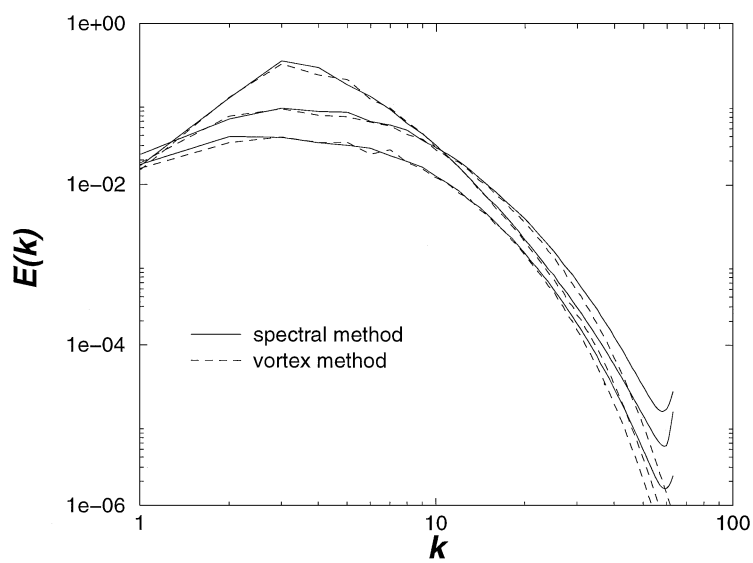

FIG. 1. Time evolution of the kinetic-energy spectra for run 1. Spectra are shown at time $t = 2$, 6, and 10 in large-eddy turnover time units.

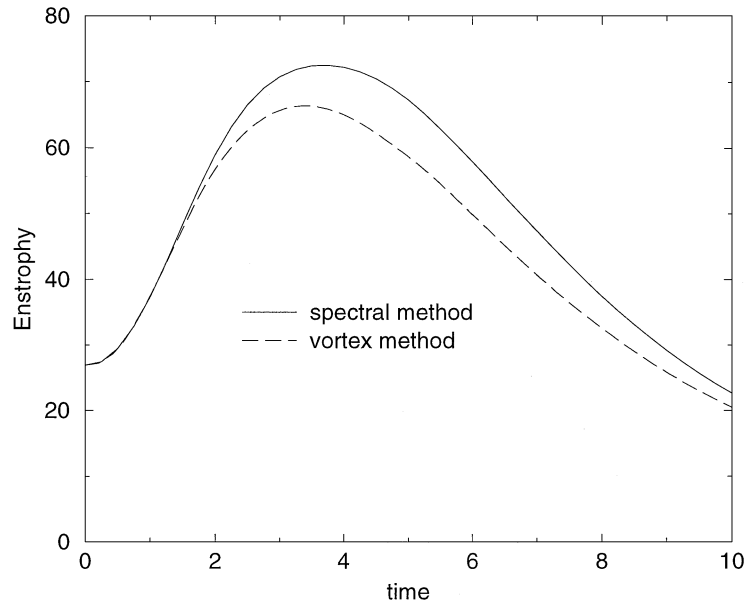

FIG. 2. Temporal evolution of the enstrophy for run 1.

2.3. *Reconnection Case (Run 2)*

We now turn to a flow which exhibits in a very clear and localized way some typical three-dimensional features (vorticity increase and topology change, production of small scales). The initial condition consists of two antiparallel vortex tubes subject to a sinusoidal perturbation. We have chosen the same initial condition as in Ref. [10]. More precisely, the

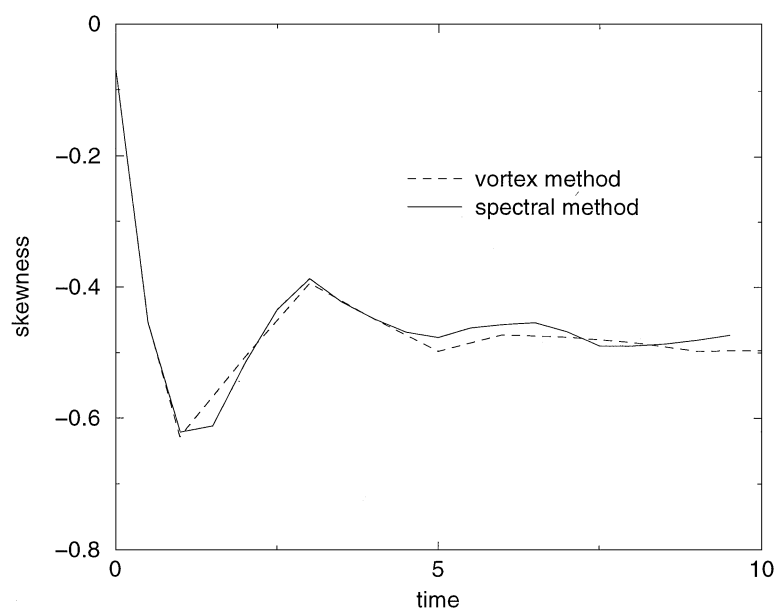

FIG. 3. Skewness factor of $-\partial u_1/\partial x_1$ for run 1.

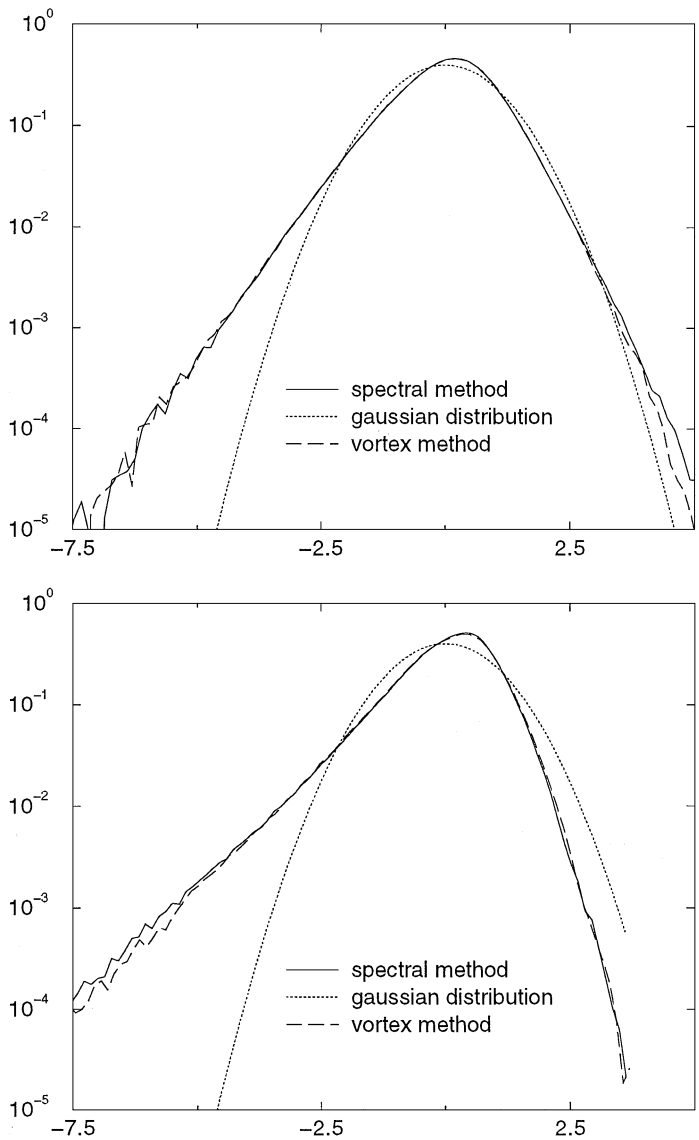

FIG. 4. Pdf of $-\partial u_1/\partial x_1$ (top) and p (bottom) for run 1.

vortex core inside each tube is given by the formula

$$\omega(r) = \begin{cases} 0 & \text{if } r > 2/3, \\ -2[1 - f(3r/2)] & \text{if } r \leq 2/3, \end{cases}$$

where

$$f(r) = \exp\left[-\frac{K}{r}\exp\frac{1}{r-1}\right]; \; K = 0.5\exp(2)\ln(2).$$

The tubes' centerlines are cosine waves of amplitude 0.5 at an angle of $\pi/3$ and a distance of 1.73 in a periodic $[0, 2\pi]^3$ box.

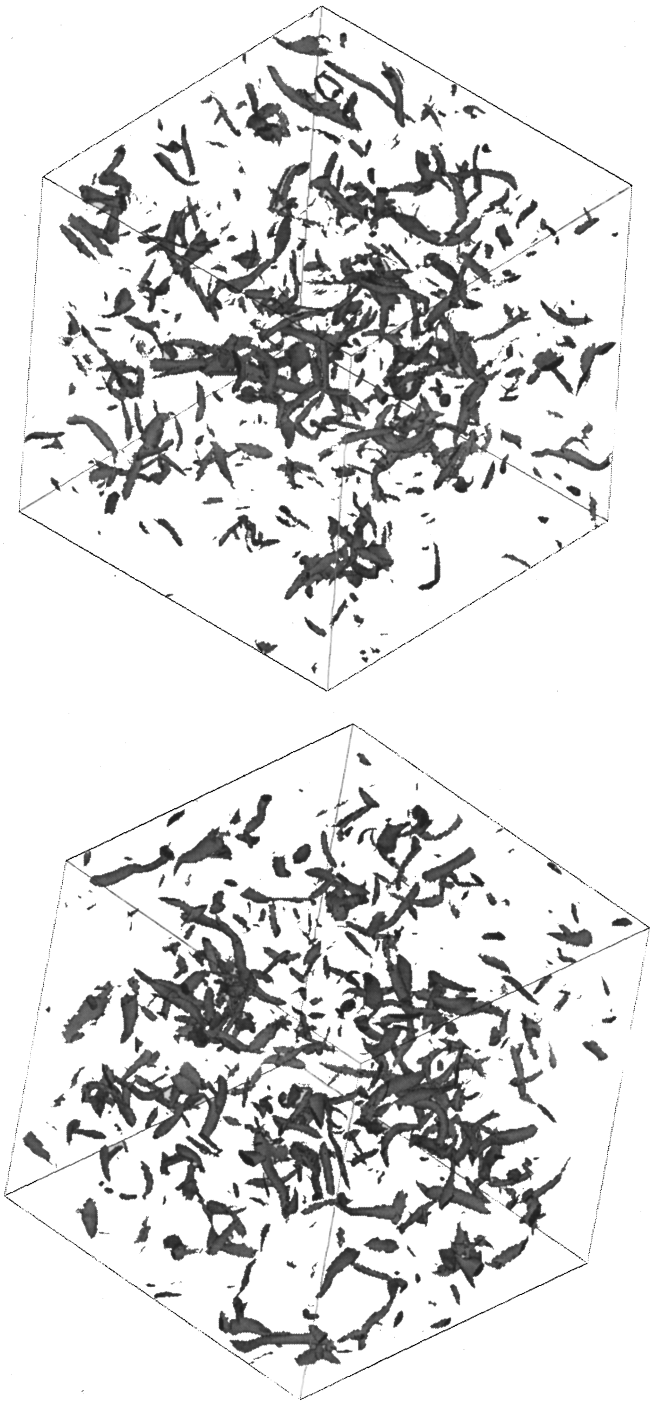

FIG. 5. Isosurface of vorticity magnitude at $t = 5$ in large-eddy turnover time units for run 1. (Top) Spectral method, (bottom) vortex method.

Reference [10] contains a precise account of the reconnection phenomena that take place for this flow. For Reynolds numbers up to 3500, a pseudospectral method is used with a refined collocation grid near the reconnection plane, giving a local resolution corresponding to a uniform grid of 640^3. We were here interested in the effect of underresolution on the results of the simulations and have run the spectral and vortex codes on 120^3 and 180^3 uniform grids for a Reynolds number of 3500.

It is well-known that underresolved spectral simulations exhibit unphysical accumulation of energy in the tail of the spectrum. The classical cure for that is to use dealiasing techniques and/or complement molecular viscosity by subgrid scale models which enforce dissipation of energy at high wavenumbers. Note that in this case the flow is laminar and not turbulent and it is more appropriate to see subgrid models as artificial viscosity techniques. Figure 6 shows the level curves of the vorticity at nondimensionalized time $t = 2$ (reconnection time is about $t = 1.5$) for the 180^3 vortex simulation, the 120^3 vortex simulation, and two different implementations of the 120^3 spectral code: one with dealiasing and one with a Smagorinsky subgrid dissipation model with a coefficient value of $C_S = 0.23$. These plots indicate that in all cases the spectral code produces spurious vorticity. As for the vortex code, it gives reasonably well-converged results for the scales that are resolved. In Fig. 7, we show the

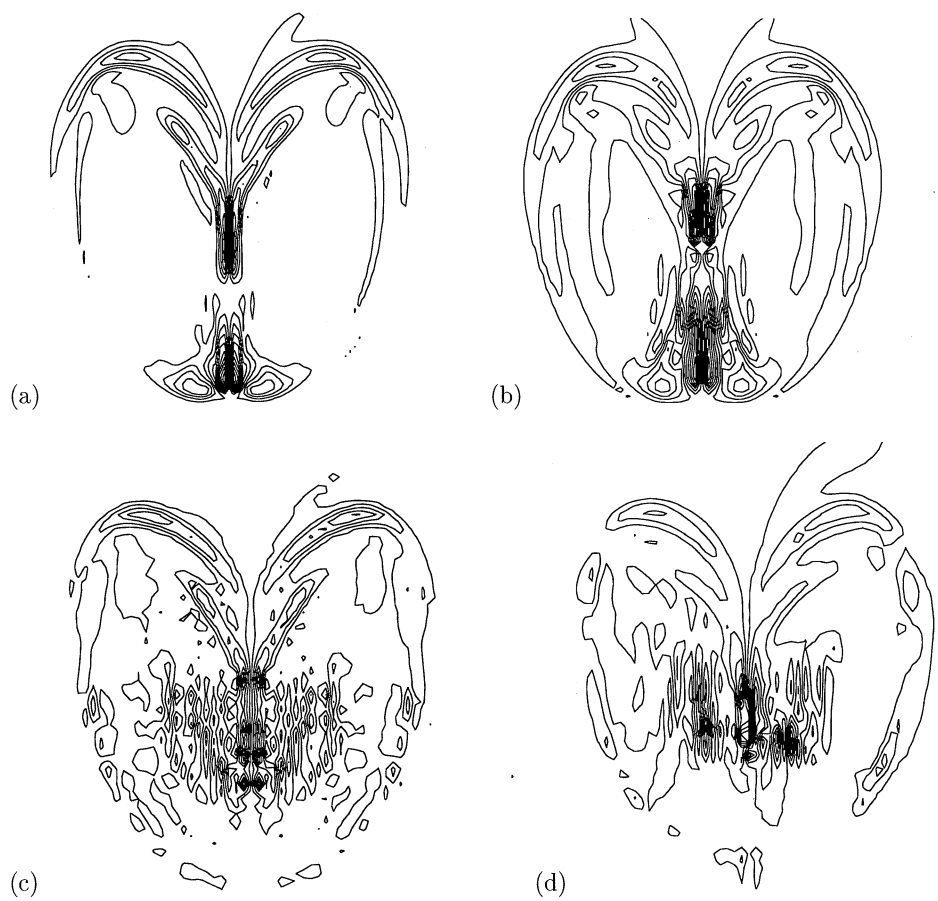

FIG. 6. Cross section of the vorticity after reconnection of the symmetry plane perpendicular to the tubes for run 2. (a) Vortex method, $N = 180$; (b) vortex method, $N = 120$; (c) dealiased spectral method, $N = 120$; (d) Smagorinsky spectral method, $N = 120$.

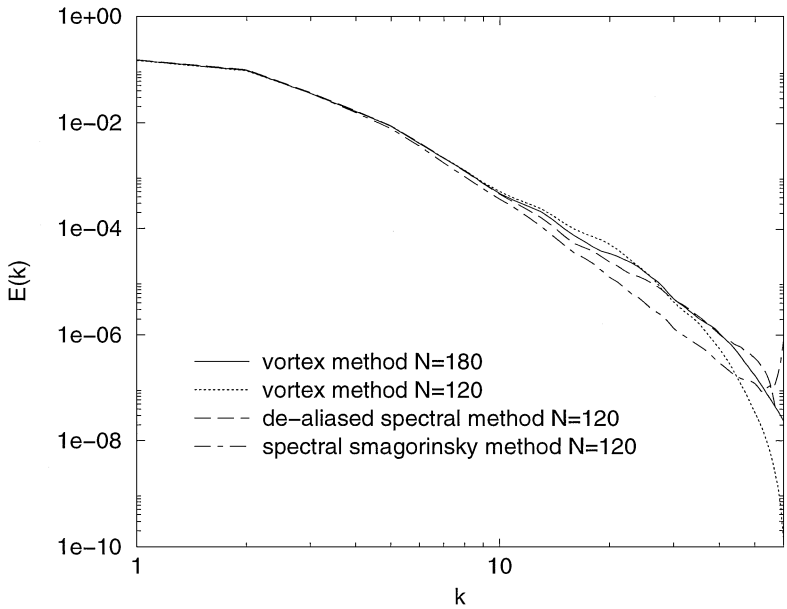

FIG. 7. Energy spectra in the direction perpendicular to the reconnection plane for run 2 at time $t = 2$.

spectra in the direction perpendicular to the reconnection plane (that is, if x is this direction, $k_x \to \sum_{k_y,k_z} |\hat{u}(k_x, k_y, k_z)|^2$). As could be expected, the spurious vortices observed in the spectral results translate into an accumulation of energy in the highest wavenumbers. More surprising, the vortex scheme avoids this problem, but not at the expense of an undesired dissipation: a comparison of the spectra with the more resolved calculation shows that it fairly resolves the smallest scales. These observations are confirmed by inspecting the enstrophy curve in Fig. 8. The curve corresponding to the vortex run actually shows a slight

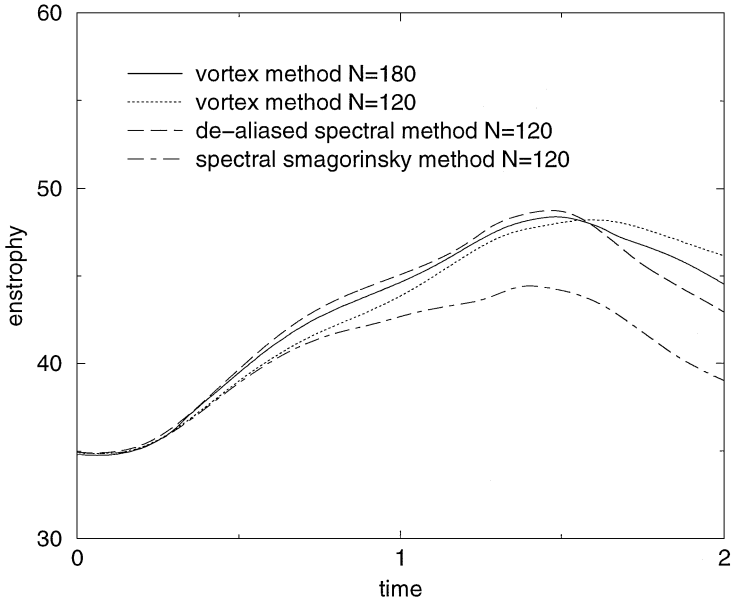

FIG. 8. Enstrophy curves for run 2.

overestimation of the enstrophy, while the dealiased spectral method exhibits an accelerated decay of the enstrophy passed the reconnection time, probably due to the intense dissipation taking place in the spurious small scales produced in the course of the calculation. As for the Smagorinsky model, it is at the same time too dissipative in the large scales and not enough in the small scales.

3. CONCLUSIONS

We have presented a comparison of the results obtained by spectral and vortex methods for two flows of interest. In the context of direct numerical simulations, that is when all scales in the inertial range and in a portion of the dissipation range are well resolved, the spectral method is more accurate in the highest wavenumbers. However, the accuracy of the vortex method in the large and intermediate scales is good enough to yield acceptable statistics. In the underresolved case, vortex methods appear to behave as accurate LES models in the sense that they avoid accumulation of energy at the end of the spectrum, without excessive dissipation in the resolved scales (the particular role played by particle methods in the context of large-eddy simulations can indeed be understood by numerical analysis, see Refs. [3–5]).

Another important issue that must be addressed when comparing two numerical methods is their computational cost. The flows that we have considered here were chosen in view of their typical 3D features and the fact that both methods were straightforward to implement in a periodic geometry. They correspond to boundary conditions for which spectral methods are obviously optimally fast, while it is clear that vortex methods are better suited to wake-type flows in which vorticity is more localized. When particles completely fill the domain (which is the case in run 1), a typical CPU time for the vortex code is 40 s for one iteration on a 128^3 grid (recall that grid and particle spacing are equal), compared to about 20 s for our spectral code (on an Alpha single-processor workstation). The computational overhead in the vortex method results from the interpolation formulas that are involved at several stages of the algorithm. For run 1, at this grid size results were converged for the vortex method for a time step $\Delta t = \|\boldsymbol{\omega}\|^{-1}$ and for the spectral method for a CFL number of 1. This gave at the beginning of the simulations a time step about five times larger for the vortex method than for the spectral method. At time 4, when vorticity reaches its peak value, time steps were roughly equal. Overall, this led to similar computational costs for the two codes (8000 and 10,000 s, respectively, for the vortex and spectral codes, up to $t = 4$). For run 2, to obtain converged results, at the given resolution, the time step of the vortex code had to be reduced to $\Delta t = 0.25\|\omega\|^{-1}$, and the overall CPU time for the vortex code was twice that of the spectral code.

Although a complete discussion of implementation issues for both methods is beyond the scope of this paper, let us also mention that in many practical situations, the treatment of boundaries may affect these figures. In a spectral code, no-slip boundary conditions often dictate the use of a Legendre-type method, for which FFTs are not available, which substantially increases the cost of the method. In a vortex method, no-slip boundary conditions are enforced by vorticity flux-type algorithms [5], which concern a few layers of particles around the boundary and thus only marginally add to the overall cost of the method. **Au: change okay?**

Given a flow and an affordable grid size, accuracy and cost considerations must be carefully balanced when it comes to the choice of a particular method and we hope that the

present comparisons may help to evaluate the strengths and limitations of vortex methods for the simulations of three-dimensional complex flows.

REFERENCES

1. C. Canuto, M. Y. Hussaini, A. Quarteroni, and T. A. Zang, *Spectral Methods in Fluid Dynamics* (Springer-Verlag, Berlin/NewYork, 1987).
2. J. P. Christiansen, Vortex methods for flow simulation, *J. Comput. Phys.* **13**, 363 (1973).
3. G.-H. Cottet, Artificial viscosity models for vortex and particle methods, *J. Comput. Phys.* **127**, 299 (1996).
4. G.-H. Cottet, *Anisotropic Subgrid-Scale Numerical Schemes for Large Eddy Simulations of Turbulent Flows*, preprint (1997).
5. G.-H. Cottet and P. Koumoutsakos, *Vortex Methods: Theory and Practice* (Cambridge Univ. Press, Cambridge, UK 2000).
6. M. Lesieur, *Turbulence in Fluids* (Kluwer, Dordrecht, 1997), 3rd ed.
7. N. N. Mansour and A. A. Wray, Decay of isotropic turbulence at low Reynolds number, *Phys. Fluids* **6** (2), 808 (1994).
8. M. L. Ould-Salihi, *Couplage de Méthodes Numériques en Simulation Directe d'Écoulements Incompressibles*, Ph.D. thesis (Université Joseph Fourier, 1998).
9. M. L. Ould-Salihi, G.-H. Cottet, and M. El Hamraoui, Blending finite-difference and vortex methods for incompressible flow computations, *SIAM J. Sci. Comput.* **22**, 1655 (2000).
10. M. L. Shelley, D. I. Meiron, and S. A. Orszag, Dynamical aspects of vortex reconnection of anti-parallel vortex tubes, *J. Fluid Mech.* **246**, 613 (1993).
11. G. Vanderlinden, *Simulation de Turbulence par Méthode Particulaire*, International Report (LMC–IMAG, 1998).